Automatic Measurement of Temporalis Muscle Thickness in Computed Tomography Head Scans

Dana Marcela Cotes Cala and Kevin Sebastián Rueda Muñoz

Degree work presented as a requirement to qualify for the title of Electronic Engineer

Advisor

Said David Pertuz Arroyo

Doctor in Engineering

Universidad Industrial de Santander

Facultad de Ingenierías Fisicomecánicas

Escuela de Ingenierías Eléctrica, Electrónica y de Telecomunicaciones

Electronic Engineering

Bucaramanga

2026

Table of Contents

Page

List of Figures

Page

List of Tables

Page

Resumen

Título: Medición automática del grosor del músculo temporal en tomografías computarizadas de cabeza*

Autor: Dana Marcela Cotes Cala y Kevin Sebastián Rueda Muñoz**

Palabras Clave: Espesor del Músculo Temporal, Tomografía Computarizada, Procesamiento de Imágenes Médicas, Medición Automática, Biomarcadores de Imagen.

Descripción:

La evaluación del estado muscular ha surgido como un biomarcador clínicamente relevante del estado nutricional, la sarcopenia y el pronóstico. Aunque la tomografía computarizada (TC) abdominal y la resonancia magnética (RM) se utilizan comúnmente para la evaluación muscular, el grosor del músculo temporal (TMT) medido en TC craneal ha ganado reconocimiento como marcador sustituto, particularmente en pacientes neurológicos. La medición manual del TMT requiere tiempo y está sujeta a variabilidad interobservador, lo que limita su uso rutinario. Presentamos una *pipeline* completamente automatizada para la cuantificación del TMT a partir de volúmenes tridimensionales de TC craneal. El marco metodológico integra una reorientación craneal basada en análisis de componentes principales, la selección del corte axial mediante puntos de referencia oculares con un desplazamiento derivado estadísticamente, la segmentación determinista del músculo temporal y la estimación geométrica de su grosor. A diferencia de los métodos basados en aprendizaje automático, el enfoque se fundamenta exclusivamente en restricciones anatómicas y geométricas explícitas, garantizando explicabilidad y reproducibilidad. La evaluación en 103 casos independientes de prueba demostró una alta concordancia con las mediciones realizadas por expertos, obteniendo un error absoluto mediano de 1.09 mm (RIC: 0.62–1.68 mm) para el TMT y de 1.92 mm (RIC: 1.21–2.73 mm) para la posición del corte. Estos resultados se encuentran dentro del rango de variabilidad interobservador reportado para la evaluación manual. Por lo tanto, la *pipeline* propuesta permite una medición estandarizada, reproducible y completamente automatizada del TMT, facilitando su integración como biomarcador cuantitativo de imagen en los flujos de trabajo clínicos.

---

* Trabajo de Grado.

** Facultad de Ingenierías Fisicomecánicas. Escuela de Ingenierías Eléctrica, Electrónica y de Telecomunicaciones. Ingeniería Electrónica. Director: Said David Pertuz Arroyo. Doctor en Ingeniería.

Abstract

Title: Automatic Measurement of Temporalis Muscle Thickness in Computed Tomography Head Scans*

Author: Dana Marcela Cotes Cala and Kevin Sebastián Rueda Muñoz**

Keywords: Temporalis Muscle Thickness, Computed Tomography, Medical Image Processing, Automated Measurement, Imaging Biomarkers.

Description:

Assessment of muscle status has emerged as a clinically relevant biomarker of nutritional condition, sarcopenia, and prognosis. While abdominal CT and MRI are commonly used for muscle evaluation, temporalis muscle thickness (TMT) measured on cranial CT has gained recognition as a surrogate marker, particularly in neurological patients. Manual TMT measurement is time-consuming and subject to interobserver variability, limiting its routine use. We present a fully automated pipeline for TMT quantification from three-dimensional cranial CT volumes. The framework integrates principal component analysis–based cranial reorientation, axial slice selection using ocular landmarks with a statistically derived offset, deterministic segmentation of the temporalis muscle, and geometric estimation of thickness. Unlike learning-based methods, the approach relies exclusively on explicit anatomical and geometric constraints, ensuring explainability and reproducibility. Evaluation on 103 independent test cases demonstrated close agreement with expert measurements, yielding a median absolute error of 1.09 mm (IQR: 0.62–1.68 mm) for TMT and 1.92 mm (IQR: 1.21–2.73 mm) for slice position. These results fall within the range of interobserver variability reported for manual assessment. The proposed pipeline therefore enables standardized, reproducible, and fully automated TMT measurement, supporting its integration as a quantitative imaging biomarker in clinical workflows.

---

* Bachelor Thesis.

** School of Physical-Mechanical Engineering. Department of Electrical, Electronics and Telecommunications Engineering. Electronic Engineering. Advisor: Said David Pertuz Arroyo. Doctor in Engineering.

Introduction

The temporalis muscle is an anatomical structure located in the lateral region of the skull, whose primary function is the elevation and retraction of the mandible during mastication (Standring, 2005). Its clinical evaluation is relevant across multiple medical disciplines, including dentistry, neurology, and intensive care medicine, where alterations in temporalis muscle thickness (TMT) have been associated with bruxism, temporomandibular disorders, sarcopenia, and neuromuscular degeneration (Lee et al., 2021; Maskos et al., 2022).

In recent years, TMT has gained increasing attention as a quantitative imaging biomarker of nutritional status, sarcopenia, and prognosis in many diseases. Several studies have demonstrated that reduced TMT is correlated with skeletal muscle mass and is associated with poor clinical outcomes, including increased mortality and functional impairment, particularly in critically ill and older patients (Maskos et al., 2022; Pesonen et al., 2025). Consequently, reliable and reproducible measurement of the temporalis muscle could become an important component of clinical assessment and longitudinal monitoring.

TMT is measured manually on axial computed tomography (CT) head slices, a process that is time-consuming and prone to interobserver variability. To address these limitations, recent research has explored automated and semi-automated approaches for temporalis muscle quantification, including image processing and machine learning-based methods (Zapaishchykova et al., 2023).

1. Problem Statement

The temporalis muscle plays a key role in mandibular biomechanics and contributes significantly to human masticatory force (Korfage et al., 2005; Standring, 2005). Clinically, its assessment is relevant for the diagnosis and monitoring of temporomandibular disorders, bruxism, and muscle atrophy conditions in elderly individuals (Okeson, 2019). In oncological and neurological populations, reduced TMT has been associated with increased risk of malnutrition, frailty, and worse clinical outcomes (Lee et al., 2021; Muglia et al., 2021). Accurate measurement of temporalis muscle thickness enables quantification of its functional status, detection of lateral muscle asymmetries, and monitoring of response to therapeutic interventions such as physical therapy or neuromuscular rehabilitation (Zapaishchykova et al., 2023). In neurological contexts, lower TMT values have been associated with increased mortality risk and prolonged disability after acute neurological events (Steindl et al., 2020).

In clinical practice, the temporalis muscle has traditionally been measured through visual inspection or with the aid of medical imaging techniques such as computed tomography (CT), magnetic resonance imaging (MRI), or ultrasound (US) (Hides et al., 2007; Nikkuni et al., 2018). Although these modalities provide valuable anatomical and functional information, most current approaches are manual and largely dependent on the operator's expertise, introducing subjectivity, interobserver variability, and limited reproducibility (Bianchi & Martinoli, 2007; Vieira & Botter, 2021). Segmentation of the temporalis muscle in axial slices is particularly challenging, as it requires accurate identification of its boundaries within a region containing multiple adjacent anatomical structures. While MRI offers excellent anatomical resolution, its cost and limited availability restrict its routine use (Matsubara et al., 2018). Ultrasound is more accessible, but its accuracy depends heavily on operator experience (Hides et al., 2007). Complementary technologies such as surface electromyography (sEMG) provide functional information but do not directly measure muscle morphology (De Luca, 1997).

In summary, measurement of temporalis muscle thickness remains largely manual, resulting in variability across professionals and institutions. Although imaging-assisted methods exist, standardized and automated quantification remains a challenge in terms of accessibility and consistency. Therefore, a more objective solution is needed to reduce human error and facilitate implementation across clinical environments.

In response to these limitations, this work proposes the development of a computational solution based on image processing techniques applied directly to three-dimensional computed tomography scans. The proposed tool will integrate modules for anatomical reorientation, optimal axial slice selection, automated tissue segmentation, and quantitative measurement of temporalis muscle thickness.

2. Objectives

2.1 General Objective

To develop an automated computational tool for estimating the thickness of the temporal muscle from three-dimensional computed tomography images of the head.

2.2 Specific Objectives

1. To implement an algorithm to perform anatomical reorientation of the skull and automatic selection of the optimal axial slice in three-dimensional computed tomography scans.

2. To design an algorithm to automatically segment the temporal muscle and associated bony structures, including the removal of unwanted artifacts.

3. To develop an automated system to estimate the thickness of the temporal muscle from the obtained segmentation and visualize the measurement results.

4. To evaluate the performance of the proposed tool using quantitative metrics comparing muscle thickness measurements obtained by experts.

3. Theoretical Framework

3.1 Fundamentals of Computed Tomography

Computed Tomography (CT) is a tomographic imaging modality that reconstructs cross-sectional anatomical representations from multiple X-ray projections acquired around the patient. Unlike conventional radiography, CT provides quantitative volumetric data in which each voxel encodes a normalized estimate of the tissue's linear attenuation coefficient. This quantitative nature enables objective tissue characterization and morphometric analysis, forming the foundation of the proposed automated TMT estimation framework.

3.1.1 X-ray Attenuation and Tomographic Reconstruction

CT imaging is based on the interaction of X-ray photons with biological tissues. As photons traverse matter, their intensity decreases according to the linear attenuation coefficient μ, which depends on tissue composition and photon energy. In the diagnostic energy range, attenuation is primarily governed by photoelectric absorption and Compton scattering (Bushberg et al., 2012). According to the Beer–Lambert law, the relationship between the incident intensity I_0 and the transmitted intensity I after traversing a thickness x is defined by $I = I_0 e^{-\mu x}$.

During acquisition, projections are collected at multiple angular orientations. Each projection corresponds to a line integral of the attenuation coefficient distribution, mathematically represented by the Radon transform $p(\theta, t) = \int \mu(x, y)\, ds$ (Kak & Slaney, 2001). Image reconstruction consists of estimating the spatial distribution $\mu(x, y, z)$ from these projections, typically using Filtered Back Projection or iterative reconstruction techniques in modern CT systems (Hsieh, 2009).

The resulting reconstructed volume is discretized into voxels, where each voxel intensity represents the average attenuation coefficient within a finite three-dimensional element. Consequently, every voxel value serves as a physically meaningful estimate of tissue attenuation, providing the basis for quantitative anatomical analysis.

3.1.2 Hounsfield Units and Tissue Characterization

To ensure standardization across scanners and acquisition protocols, attenuation values are expressed in Hounsfield Units (HU). This normalization allows reproducible tissue characterization and enables deterministic threshold-based segmentation strategies. The HU scale is defined relative to water attenuation as shown in Eq. 1 (Bushberg et al., 2012).

$$HU = 1000\frac{\mu - \mu_{\text{water}}}{\mu_{\text{water}}} \tag{1}$$

By definition, water corresponds to 0 HU and air to approximately -1000 HU. In cranial CT imaging, adipose tissue typically ranges around -100 HU, skeletal muscle between 30–60 HU, and cortical bone above 300 HU. Because the proposed segmentation algorithm relies directly on predefined HU intervals to differentiate bone and temporalis muscle, the HU scale constitutes the physical basis for automated tissue classification.

3.1.3 Spatial Representation in DICOM

CT volumes are stored using the Digital Imaging and Communications in Medicine (DICOM) standard, which encodes both voxel intensity data and spatial metadata necessary for geometric interpretation (Clunie, 2016). Relevant attributes include Pixel Spacing $(\Delta x, \Delta y)$, Slice Thickness (Δz), Image Position (Patient), and Image Orientation (Patient), the latter defined through direction cosines. Voxel space refers to the discrete index-based coordinate system defined by integer indices (i, j, k), whereas physical space corresponds to real-world millimeter coordinates (x, y, z).

Accurate morphometric measurements require explicit conversion from voxel space to physical space. This mapping is described by an affine transformation expressed in homogeneous coordinates as $[x, y, z, 1]^T = \mathbf{M}[i, j, k, 1]^T$, where $\mathbf{M}$ is a 4×4 matrix constructed from voxel spacing, orientation direction cosines, and the image origin. By integrating these spatial parameters, the formulation ensures spatial consistency during volume reorientation and precise geometric measurement.

3.2 Anatomical Coordinate Systems

Medical images are interpreted within anatomical reference systems that define spatial orientation relative to the patient. The two most common conventions are the LPS (Left–Posterior–Superior) and RAS (Right–Anterior–Superior) coordinate systems (Clunie, 2016). Anatomical planes are defined as sagittal (left–right division), coronal (anterior–posterior division), and axial (superior–inferior division). Correct identification of these planes is essential for cranial reorientation, lateralization.

3.3 Spatial Transformations in Medical Imaging

Cranial reorientation requires mathematical transformations that modify the spatial reference frame while preserving anatomical integrity. These transformations are fundamental for aligning volumes prior to automated analysis.

3.3.1 Rigid Transformations

Rigid transformations consist of rotations and translations and preserve distances and angles. In three-dimensional space, rigid motion has six degrees of freedom: three rotational and three translational parameters. The transformation of a point $\mathbf{x}$ under a rigid motion is defined as $\mathbf{x}' = \mathbf{R}\mathbf{x} + \mathbf{t}$ (Foley et al., 1996), where $\mathbf{R}$ is a rotation matrix and $\mathbf{t}$ is a translation vector. This formulation allows for precise cranial alignment without introducing geometric distortion.

3.3.2 Affine Transformations

Affine transformations extend rigid transformations by incorporating scaling and shearing. They are represented in homogeneous coordinates using a 4×4 matrix, enabling composition of multiple transformations into a single operation (Foley et al., 1996). This representation underlies the computational implementation of volume reorientation.

3.3.3 Rotation Matrices

Rotation matrices are orthogonal matrices satisfying $\mathbf{R}^\top \mathbf{R} = \mathbf{I}$ and $\det(\mathbf{R}) = 1$. These properties ensure preservation of Euclidean distances and orientation. Rotation matrices can be interpreted as change-of-basis operators, allowing alignment of anatomical axes with principal geometric directions.

3.3.4 Principal Component Analysis (PCA)

Principal Component Analysis (PCA) is a statistical method used to identify orthogonal directions of maximum variance in a dataset (Jolliffe, 2002). Given a set of 3D points representing cranial bone voxels, the covariance matrix is defined as shown in Eq. 2.

$$\mathbf{\Sigma} = \frac{1}{N} \sum_{i=1}^{N} (\mathbf{x}_i - \bar{\mathbf{x}})(\mathbf{x}_i - \bar{\mathbf{x}})^\top \tag{2}$$

The eigenvectors of $\mathbf{\Sigma}$ define the principal axes, while the eigenvalues represent variance along those axes. In this work, PCA provides an automatic, annotation-independent method for cranial alignment by aligning principal axes of bone distribution with canonical coordinate axes.

3.4 Cranial Reorientation Strategies

Automated cranial reorientation aims to align head CT volumes into a consistent anatomical reference frame prior to quantitative analysis. Different methodological approaches have been proposed in the literature. Landmark-based methods rely on manually or automatically identified anatomical reference points, such as the anterior commissure or orbital landmarks. Although effective, these methods depend on accurate detection and may be sensitive to anatomical variability or pathological alterations.

Deep learning approaches learn alignment directly from labeled datasets. While potentially powerful, they require large annotated datasets, may lack interpretability, and can exhibit reduced generalization when imaging protocols vary. Global geometric methods operate directly on

spatial distributions of anatomical structures, typically bone. These approaches are annotation-independent, reproducible, and computationally efficient. In this work, Principal Component Analysis (PCA) is selected because it aligns the volume according to intrinsic geometric variance, does not require manual annotation, and provides an interpretable mathematical solution.

3.5 Automatic Axial Slice Selection

Accurate temporalis muscle thickness measurement requires identification of a clinically standardized axial plane. The automated selection of this slice must therefore be anatomically grounded and geometrically robust.

3.5.1 Anatomical Basis for TMT Measurement

Clinically, temporalis muscle thickness is measured at a standardized axial level commonly corresponding to the orbital roof or superior orbital region, depending on institutional protocols. This level provides reproducible visualization of the temporalis muscle belly while minimizing variability due to cranial tilt or inferior anatomical structures. The automated approach must replicate this anatomical reference to ensure comparability with manual radiological measurements.

3.5.2 Circular Structure Detection

The orbital cavities exhibit approximately circular cross-sectional geometry in axial CT slices. Automatic identification of these structures can be formulated as a circle detection problem. The Hough Transform provides a parametric method for detecting circular shapes by mapping edge points into a parameter space defined by center coordinates and radius (Duda & Hart, 1972). In Cartesian coordinates, a circle is defined by the expression $(x - a)^2 + (y - b)^2 = r^2$, where (a, b) represents the center and r the radius. Detection of these bilateral orbital structures enables precise anatomical localization of the axial reference plane.

3.5.3 Statistical Offset Modeling

Because anatomical variability exists between patients, the final axial measurement plane may require a controlled offset relative to detected orbital landmarks. Statistical modeling using sample mean and standard deviation provides a robust estimation of this displacement. Given a set of slice indices z_i, the mean axial level and its variability are defined as shown in Eq. 3 and Eq. 4, respectively:

$$\bar{z} = \frac{1}{N}\sum_{i=1}^{N} z_i \qquad (3) \qquad\qquad \sigma = \sqrt{\frac{1}{N}\sum_{i=1}^{N}(z_i - \bar{z})^2} \qquad (4)$$

This statistical framework improves robustness against inter-patient anatomical variability and imaging differences.

3.6 CT-Based Muscle Segmentation

Accurate measurement of temporalis muscle thickness requires reliable isolation of the muscle region from surrounding tissues. Segmentation in CT leverages intensity-based and spatial connectivity properties.

3.6.1 Threshold-Based Segmentation

Threshold-based segmentation classifies voxels according to intensity ranges derived from Hounsfield Units. Since skeletal muscle exhibits characteristic HU values between approximately 30–60 HU, binarization is defined as $B(x) = 1$ if $HU_{\min} \leq HU(x) \leq HU_{\max}$, and 0 otherwise. This deterministic approach directly exploits the physical interpretation of voxel intensity to isolate specific tissue types based on their attenuation properties.

3.6.2 Connected Component Analysis

Binary segmentation may include multiple disjoint regions. Connected component analysis identifies spatially contiguous voxel clusters using defined neighborhood connectivity (4- or 8-connectivity in 2D; 6-, 18-, or 26-connectivity in 3D) (Gonzalez & Woods, 2018). The labeling

process assigns a unique identifier to each connected region, enabling selection of anatomically relevant components based on size and location.

3.7 Geometric Estimation of Muscle Thickness

Quantitative thickness measurement requires formal geometric definition in continuous physical space.

3.7.1 Euclidean Distance in Physical Space

The Euclidean distance between two points in three-dimensional space is defined as $d = \sqrt{(x_2 - x_1)^2 + (y_2 - y_1)^2 + (z_2 - z_1)^2}$. To ensure geometrically accurate morphometric measurements, all computations are performed in millimeter coordinates obtained from DICOM spatial metadata. This conversion from pixel indices to physical space is essential for maintaining the scale and orientation consistency required in clinical analysis.

3.7.2 Orthogonal Thickness Computation

Muscle thickness is defined as the minimum perpendicular distance between two opposing boundary surfaces. Given a boundary curve parameterized as $\mathbf{r}(s)$, the tangent vector is $\mathbf{t}(s) = \frac{d\mathbf{r}}{ds}$, and the normal vector $\mathbf{n}(s)$ is orthogonal to $\mathbf{t}(s)$. Thickness is computed as the minimal projection of boundary points along $\mathbf{n}(s)$, where the formal condition of orthogonality is defined by the inner product $\mathbf{t} \cdot \mathbf{n} = 0$. This geometric formulation ensures that the thickness measurement remains independent of any orientation bias.

3.8 Statistical Evaluation Metrics

Quantitative validation of the automated method requires statistical comparison with the clinical reference. The absolute error between automated and manual measurements is defined as $E = |T_{\text{auto}} - T_{\text{manual}}|$, where Mean Absolute Error (MAE), median error, and interquartile range (IQR) provide measures of central tendency and dispersion. Furthermore, correlation strength is assessed

using Pearson's correlation coefficient r, defined by the ratio of the covariance of the variables to the product of their standard deviations (Altman, 1991).

$$r = \frac{\sum(x_i - \bar{x})(y_i - \bar{y})}{\sqrt{\sum(x_i - \bar{x})^2 \sum(y_i - \bar{y})^2}} \tag{5}$$

Agreement analysis may be further evaluated using Bland–Altman methodology and intraclass correlation coefficient (ICC), which quantify bias and reproducibility in paired measurement studies (Bland & Altman, 1986).

4. Previous related work

The automatic measurement of temporal muscle thickness in CT images has gained increasing relevance as a biomarker of sarcopenia, frailty, and nutritional status (Muglia et al., 2021). This section presents a structured review of the main technical and clinical approaches.

4.1 Clinical Application of TMT as a Biomarker

TMT has been widely explored as a clinical marker of functional status and prognosis in various contexts. Pesonen et al. (Pesonen et al., 2025) established statistical reference values for TMT in CT, considering the influence of sex and age, by analyzing over 9,000 patients. These reference values are essential for establishing clinically interpretable thresholds in daily practice. In intensive care settings, Maskos et al. (Maskos et al., 2022) compared TMT measurements using CT and ultrasound in critically ill patients, finding an intraclass correlation coefficient (ICC) of 0.90 for CT measurements. Their study validated TMT as a tool for longitudinal monitoring, particularly useful in patients with fluctuating health conditions. Similarly, Mohajerani et al. (Mohajerani et al., 2025) investigated the prognostic value of TMT in patients with subarachnoid hemorrhage, finding that reduced muscle thickness after the neurological event was significantly associated with higher mortality and worse functional outcomes. These studies support the utility of TMT as a transversal indicator applicable to multiple clinical domains.

4.2 Manual and Semi-Automated Measurement

Early studies were based on manual measurement of TMT in CT or MRI images. Lee et al. (Lee et al., 2021) demonstrated that manual TMT measurement in CT predicts progression-free survival in head and neck cancer, showing high interobserver correlation (ICC $\approx$ 0.89). These findings early validated the potential of TMT as a relevant clinical marker. Cronin et al. (Cronin et al., 2020), on the other hand, proposed a semi-automated alternative in the context of ultrasound by developing a deep learning–based system capable of identifying aponeuroses and muscle fascicles.

The system achieved errors below 0.2 mm compared to human measurements, marking significant progress toward greater objectivity and reproducibility. Despite these advances, both approaches still present important limitations related to operator dependency, interobserver variability, and scalability in high-volume clinical environments.

4.3 Automatic Segmentation with Deep Learning

With the rise of deep learning, automatic solutions have been developed to overcome the constraints of manual and semi-automatic methods. Zapaishchykova et al. (Zapaishchykova et al., 2023) presented a pipeline for automatic TMT measurement in MRI using a population-based approach on over 23,876 subjects. The system enabled the generation of normalized growth curves, representing a step toward standardizing muscle morphological analysis in large cohorts. Kanavati et al. (Kanavati et al., 2020) implemented a fully convolutional neural network (FCNN) for muscle segmentation in axial CT abdominal slices, achieving Dice coefficients above 0.95, demonstrating high precision in soft tissue identification. Chen et al. (Chen et al., 2025) complemented these efforts by designing a system for the joint segmentation of muscle and adipose tissue in full-body CT scans. Their approach achieved Dice coefficients above 0.89, consolidating its utility for comprehensive body composition analysis. Finally, Soufi et al. (Soufi et al., 2024) proposed a model for the segmentation of musculoskeletal structures from hip to knee. A notable feature of their work was the integration of uncertainty estimation, a relevant metric for real clinical environments, achieving AUROC values above 0.95 and validating the tool's robustness. Although all these developments show great potential, their widespread adoption remains limited by the need for large volumes of annotated data, the architectural complexity of the models, and the associated computational demands. However, to the best of our knowledge, no previous works have addressed the problem of estimating TMT in head CT images, which is our main goal.

4.4 Geometric Reconstruction and 3D Visualization

Three-dimensional anatomical reconstruction is essential for intuitive and accurate visualization and quantification of muscle structures. The Marching Cubes algorithm, introduced by Lorensen and Cline (Lorensen & Cline, 1987), has been foundational for generating triangulated surfaces from segmented CT volumes. This technique has been adopted by clinical software such as 3DSlicer, facilitating high-resolution anatomical exploration. In an applied context, Soufi et al. (Soufi et al., 2024) demonstrated the validity of using automated volumetric segmentation combined with 3D reconstruction to measure musculoskeletal structures in CT scans from hip to knee. Their approach allowed not only accurate identification of relevant surfaces but also visualization of the entire muscle geometry in an interactive environment. These advances suggest that integrating geometric methods with reliable segmentations can be an effective path to standardizing and scaling TMT measurement in clinical practice.

4.5 Current Challenges

Automatic measurement of temporal muscle thickness faces several challenges that have limited its systematic integration into clinical environments. One of the main issues is the lack of public datasets containing validated manual segmentations of the temporal muscle in cranial CT scans. While initiatives like TotalSegmentator have made progress in multistructure segmentation in CT, they do not specifically include the temporal muscle or suitable slices for its analysis (Wasserthal et al., 2023). This gap hinders the training of robust supervised models, especially for small and anatomically variable structures. Additionally, the cranial region often presents artifacts such as dental implants or prostheses that interfere with image quality and affect precise automatic muscle segmentation (Barrett & Keat, 2004). The high interpatient variability in skull orientation and morphology also poses a major challenge for standardizing measurements.

On the other hand, current deep learning–based solutions, although promising, typically require large data volumes, complex architectures, and advanced computing resources, making implementation difficult in institutions with limited infrastructure (Bonaldi et al., 2023). Moreover, the

integration of these tools into real clinical workflows remains limited due to poor compatibility with PACS systems and standard DICOM protocols (Bonaldi et al., 2023). Additionally, while some recent approaches incorporate uncertainty estimation to enhance result reliability, their application to temporal muscle analysis remains incipient.

4.6 Contribution to the Proposed Work

The studies reviewed in the literature have been essential in guiding both the technical design and the clinical rationale of the proposed tool. For instance, the works by Pesonen et al. (Pesonen et al., 2025) and Maskos et al. (Maskos et al., 2022) highlight the clinical relevance of TMT as a reliable biomarker, reinforcing the motivation to develop automated methods for its assessment in hospital environments. Similarly, the findings of Mohajerani et al. (Mohajerani et al., 2025) on the association between reduced TMT and adverse neurological outcomes justify the need for objective, efficient, and accessible measurement approaches.

From a technical perspective, the manual and semi-automated methods described by Lee et al. (Lee et al., 2021) and Cronin et al. (Cronin et al., 2020) demonstrate the challenges of operator dependency and scalability, emphasizing the importance of automation. Building on these approaches, this work adopts their anatomical logic—such as the use of well-defined regions of interest and geometric principles—and translates them into computational methods for estimating muscle thickness.

Furthermore, studies employing deep learning and advanced segmentation techniques, such as those by Kanavati et al. (Kanavati et al., 2020), Chen et al. (Chen et al., 2025), and Zapaishchykova et al. (Zapaishchykova et al., 2023), demonstrate the strong potential of machine learning models for improving accuracy and robustness in musculoskeletal image analysis. These methods represent valuable tools that could be integrated into the project if the data, computational resources, and performance requirements make their implementation feasible. Therefore, this work remains open to leveraging both classical image processing and machine learning-based strategies to achieve reliable and adaptable automation.

In summary, inspired by proposals such as that of Soufi et al. (Soufi et al., 2024), which combine anatomical segmentation and geometric analysis for quantitative muscle assessment, this work plan aims to develop an adaptable and efficient approach for TMT estimation using CT images. The proposed methodology prioritizes clinical feasibility and computational efficiency while maintaining flexibility to incorporate advanced learning-based components as the project evolves.

5. Methodology

This study presents the development and evaluation of a fully automated pipeline for the measurement of temporalis muscle thickness (TMT) from head computed tomography (CT) scans using publicly available data. The proposed methodology is designed to operate without manual intervention, enabling reproducible, objective, and scalable TMT assessment across heterogeneous imaging datasets.

5.1 Dataset and Image Acquisition

This study was conducted using cranial computed tomography scans obtained from the publicly available CQ500 dataset (Qure.ai, 2018). This dataset consists of head CT scans acquired in routine clinical settings from patients presenting heterogeneous neurological findings. The data were collected across six radiology centers within a single metropolitan area, providing substantial variability in scanner models, acquisition protocols, patient anatomy, and imaging conditions.

No pathology-based exclusion criteria were applied. Consequently, the dataset comprises a broad spectrum of clinical conditions, ensuring a realistic representation of clinical scenarios. A total of 148 patients were included in this study, of whom 45 were assigned to the development cohort and 103 to an independent test cohort. The development cohort was employed to derive the anatomical parameters required by the proposed pipeline, whereas the test cohort was reserved exclusively for unbiased performance evaluation.

Although the proposed methodology does not rely on learning-based models, this data partitioning strategy was adopted to prevent bias in the estimation of data-driven anatomical parameters and to ensure objective evaluation of the deterministic pipeline. All images were provided in Digital Imaging and Communications in Medicine (DICOM) format and consisted of complete volumetric series suitable for three-dimensional processing. The scans exhibit variations in spatial resolution, slice thickness, and patient head positioning, accurately reflecting real-world clinical acquisition conditions.

5.2 Overview of the Proposed Pipeline

The automated pipeline for TMT measurement is structured into four main stages, as shown in Figure 1. First, a *head reorientation* is performed using Principal Component Analysis (PCA)-based position estimation to standardize the volume alignment. Second, the *slice selection stage* identifies the target axial plane by detecting the eye centers and applying a predefined vertical Z-offset. Third, the *tissue segmentation* stage generates masks for the skull and temporalis muscle. Finally, the *TMT measurement* is calculated by determining the maximum perpendicular distance from a tangential baseline within the segmented regions.

Figure 1

System overview

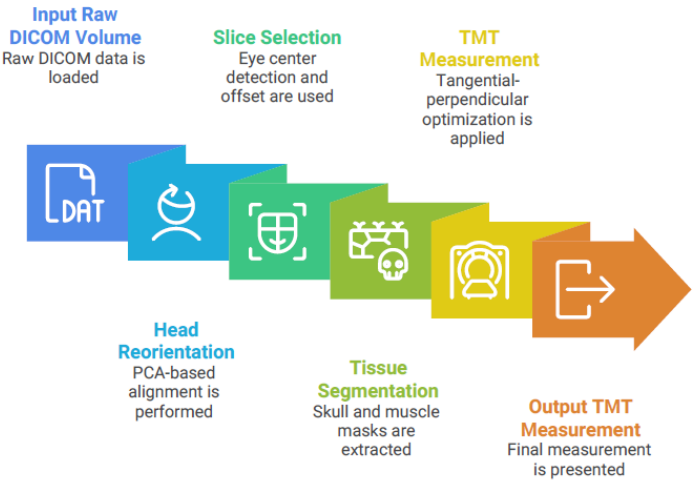

Note. System overview of the proposed automated TMT measurement workflow.

5.2.1 Head Reorientation

To reduce acquisition-dependent variability in head positioning, an automatic cranial reorientation step was applied to all CT volumes prior to axial slice selection.

High-density voxels corresponding to cranial bone were first isolated using a fixed Hounsfield unit (HU) threshold greater than 600, providing a robust representation of skull geometry. Based on the spatial distribution of these voxels, principal component analysis (PCA) was then applied

to estimate the dominant orientation of the head, from which the principal anatomical axes were derived. These axes were subsequently used to compute a global rotational transformation that was applied to the CT volume in order to standardize its anatomical alignment. This reorientation step establishes a consistent spatial reference frame across subjects, thereby improving the robustness of subsequent anatomical slice selection and temporalis muscle analysis. A representative example of the reorientation process is shown in Figure 2.

Figure 2

Automatic anatomical reorientation

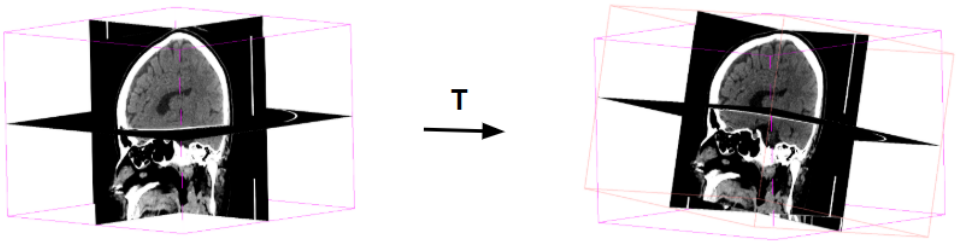

Note. Automatic anatomical reorientation applied to a head CT volume. Left: original image orientation influenced by patient positioning during acquisition. Right: standardized cranial alignment obtained after the proposed reorientation algorithm.

5.2.2 Automatic Axial Slice Selection

Accurate axial slice selection is critical for reliable temporalis muscle thickness (TMT) measurement, as small deviations along the craniocaudal axis may introduce variability in thickness estimates. To ensure anatomical consistency and reproducibility, an automatic slice selection strategy was developed based on ocular landmark detection combined with a fixed superior offset derived from experts-defined measurements.

Following anatomical reorientation, each CT volume is represented within a standardized coordinate system. Bilateral orbital cavities are automatically detected in the coronal plane and used as anatomical reference landmarks due to their high contrast and consistent anatomical appearance

in cranial CT imaging. Detection is performed using a circular shape–based approach. The centers of the left and right orbits are identified and geometrically validated, and their average vertical coordinate defines a single ocular reference level (see Figure 3b).

To determine the anatomical location typically selected for TMT assessment, axial slices manually chosen by expert readers from the 45 subjects included in the development cohort were retrospectively analyzed. For each subject, the physical distance between the reader-selected slice and the ocular reference level was computed along the craniocaudal axis. This analysis revealed a consistent anatomical preference, characterized by a mean superior displacement of 20.4 mm relative to the ocular reference level.

Based on this observation, automatic slice selection is performed by applying a fixed superior offset of 20.4 mm from the ocular reference level. The axial slice whose physical location is closest to this target position is then selected for subsequent temporalis muscle segmentation and thickness measurement. Figure 3 illustrates the two principal stages of the proposed axial slice selection strategy: automatic detection of bilateral orbital landmarks in the coronal plane and the spatial relationship between the resulting ocular reference level and the axial slice manually selected by expert readers.

5.2.3 Temporalis Muscle Segmentation

Following automatic axial slice selection, the temporalis muscle is segmented to delineate its anatomical boundaries for subsequent thickness estimation.

Segmentation is performed on the selected axial slice using fixed Hounsfield unit (HU) thresholds ranging from 20 to 200 HU in order to isolate soft tissue while suppressing air and high-density cranial bone. The resulting binary mask is then refined by connected component analysis, in which artifacts and irrelevant components are removed. Only lateral components consistent with the expected anatomical location of the bilateral temporalis muscles are retained.

In parallel, a higher HU threshold exceeding 500 HU is applied to extract a cranial bone mask from the same axial slice. This skull mask is preserved as an independent anatomical reference and

Figure 3

Automatic axial slice selection

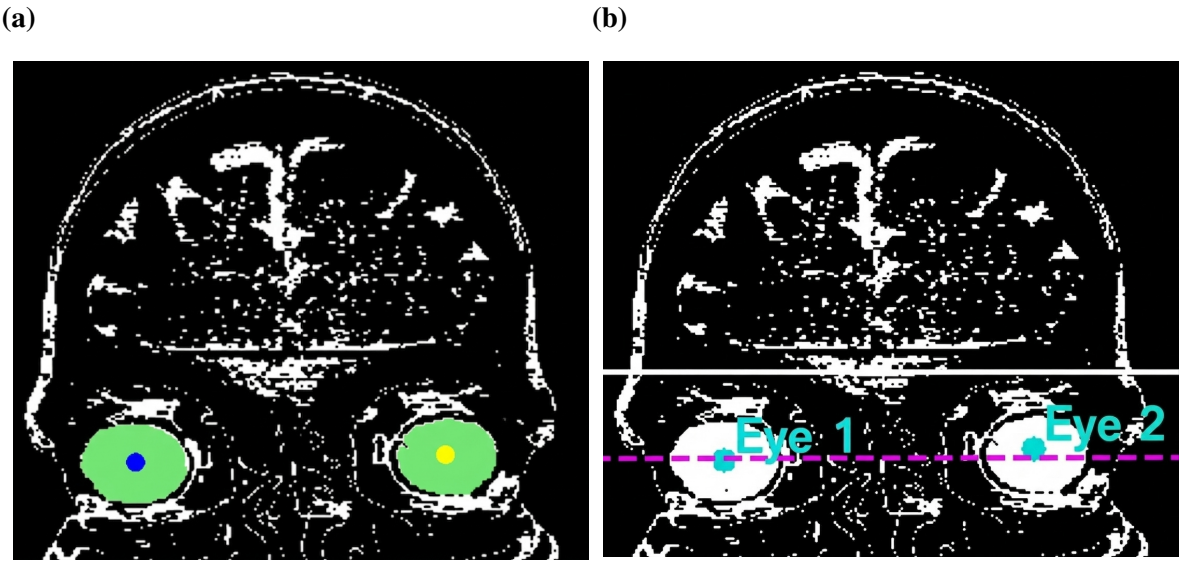

Note. Automatic axial slice selection based on ocular landmarks. (a) CT volume windowed between −20 and 20 Hounsfield units (HU) to enhance orbital cavity visualization, with detected orbital centers shown in blue and yellow. The overlay indicating the orbital cavities is rendered in green. (b) Coronal view showing the ocular reference level (magenta dashed line) and the axial slice manually selected by expert readers (solid white line).

is later used to define geometric constraints during the thickness measurement stage.

The output of this segmentation stage consists of two masks: (i) bilateral temporalis muscle masks and (ii) a cranial bone mask. Representative results of the segmentation process are presented in Figure 4.

5.2.4 Temporalis Muscle Thickness Measurement

After temporalis muscle segmentation, a deterministic geometric strategy was applied to estimate the TMT on the selected axial slice. The measurement procedure consists of three main steps: detection of cranial landmark points, construction of tangential reference lines, and estimation of muscle thickness using perpendicular probing. This strategy is designed to emulate a standard manual measurement procedure (Pesonen et al., 2025), while ensuring reproducibility and independence from manual landmark placement.

Figure 4

Temporalis muscle segmentation

(a) **(b)** **(c)**

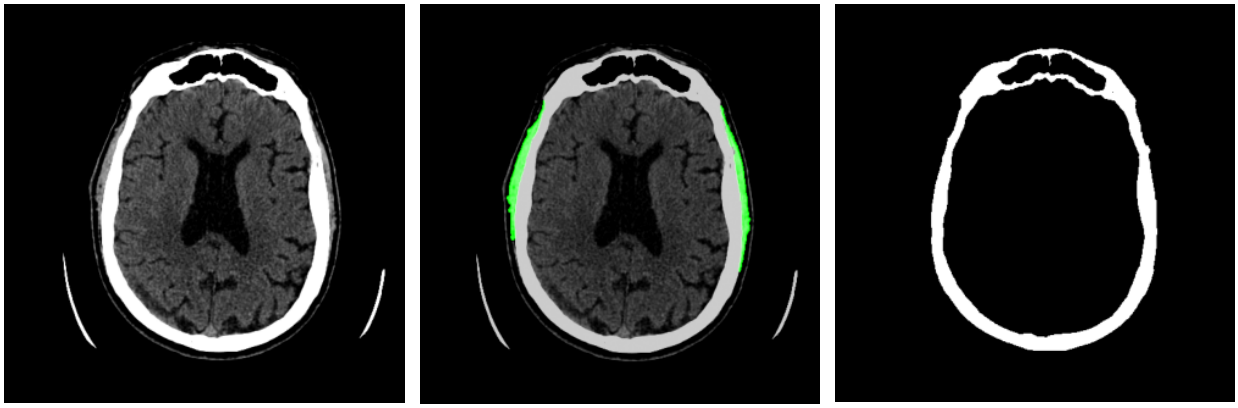

Note. Automated temporalis muscle segmentation on the selected axial CT slice. (a) Original CT image. (b) Overlay of the segmented temporalis muscle for visual validation. (c) Segmented cranial bone structures used for anatomical reference.

First, superior cranial landmark points were automatically detected on both sides of the skull contour by analyzing changes in the curvature of the superior cranial boundary. Starting from the most superior region of the cranial bone mask, the outer skull contour was scanned laterally and downward. The landmark on each side was defined as the first corner point where a pronounced downward deviation of the contour was observed, corresponding to the transition from the convex cranial surface to an inward cavity. An equivalent scanning procedure was applied in the opposite direction for the contralateral side. These points represent the most superior and lateral cranial boundaries and serve as anatomical anchors for the subsequent construction of reference geometry. Examples of the automatically detected cranial landmarks are shown in Figure 5(a).

Second, tangential reference lines were constructed for each side of the skull using the detected cranial landmarks. For each landmark, multiple candidate lines were generated by pairing the landmark with points sampled along the outer contour of the inferior cranial region. The candidate line that exhibited the minimal number of intersections with the cranial bone mask—corresponding to a near-tangential configuration—was selected. This procedure results in a tangential line that closely follows the external contour of the skull and provides a stable anatomical reference, analogous to

the orientation implicitly chosen by the reader during manual TMT assessment. The final tangential configurations for both sides are illustrated in Figure 5(b).

Finally, TMT was estimated by projecting multiple perpendicular line segments from uniformly sampled points along each tangential reference line toward the interior of the temporalis muscle region. Along each perpendicular direction, the superior and inferior muscle boundaries were detected by identifying continuous intersections with the segmented muscle mask. For each side, TMT was defined as the maximum Euclidean distance between these boundaries across all perpendicular samples. This definition mirrors clinical practice, where readers measure TMT at the location of the greatest muscle thickness. An example of boundary detection along a perpendicular probing line is shown in Figure 5(c).

Figure 5

Geometric thickness measurement procedure

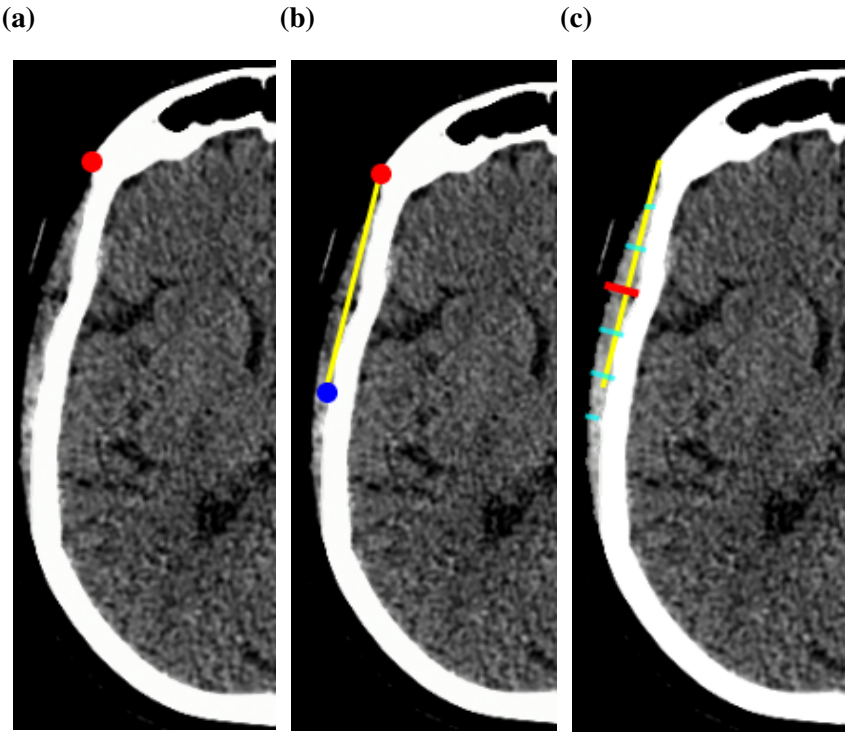

Note. Geometric procedure for automated temporalis muscle thickness estimation (right side shown for visualization clarity). (a) Automatic detection of the superior cranial landmark on the axial slice based on contour curvature analysis. (b) Construction of a tangential reference line aligned with the external skull contour. (c) Thickness estimation through perpendicular probing and muscle boundary detection.

6. Experimental Results

The pipeline was evaluated on an independent test set of cranial CT scans after all anatomical parameters had been defined using the separate development subset.

6.1 Head Reorientation

For each subject, the absolute craniocaudal (Z-axis) distance between the axial plane selected by the proposed method and the plane selected by an expert reader was computed in millimeters. Specifically, the Z-coordinate difference was calculated at all corresponding in-plane locations between both axial planes, and the resulting absolute distances were averaged to obtain a single representative misalignment value per subject, as illustrated schematically in Figure 6. This metric quantifies global axial plane misalignment and reflects the degree of anatomical consistency achieved through reorientation.

Table 1 summarizes the axial alignment discrepancies before and after automatic cranial reorientation, both measured with respect to volumes manually reoriented by expert readers.

Table 1

Axial plane distance before and after reorientation

Comparison	Median [IQR] (mm)
Original vs. Reader	12.10 [9.84 – 14.72]
Reoriented vs. Reader	9.45 [6.32 – 11.98]

Note. Absolute Z-axis distance between the reader-selected axial plane and the corresponding planes before and after automatic cranial reorientation. Values are reported as median and interquartile range (IQR).

As shown in Table 1, automatic reorientation reduces large position-induced misalignments and yields a more consistent spatial reference frame across subjects.

A qualitative visual assessment was performed to evaluate the effectiveness of the proposed cranial reorientation procedure. Figure 7 presents a representative subject with overlays in the axial, coronal, and sagittal anatomical planes.

The observed alignment of the skull contours and intracranial structures indicates that the

Figure 6

Cranial reorientation evaluation

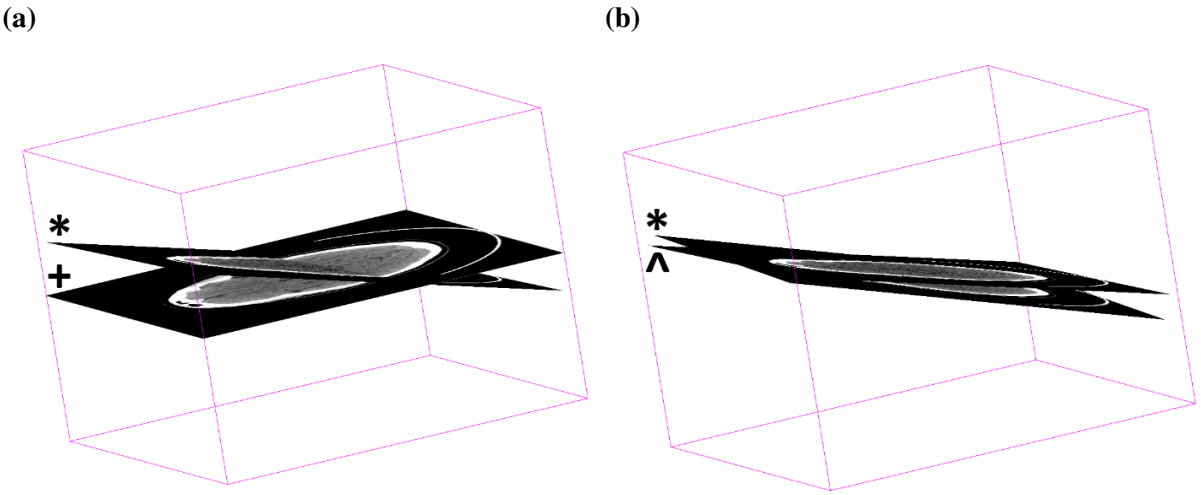

Note. Evaluation of cranial reorientation using axial plane overlays. Symbols denote plane orientation: + original acquisition, * expert reader correction, and ˆ automated correction. (a) Overlay between the original CT volume and the volume manually reoriented by the expert reader. (b) Overlay between the reader-reoriented volume and the volume reoriented using the proposed method, demonstrating improved anatomical alignment and reduced positioning variability.

proposed reorientation strategy reproduces the anatomical position established by the reader.

6.2 Automatic Axial Slice Selection

The performance of the automatic axial slice selection stage was quantitatively evaluated by comparing the craniocaudal position of the slice selected by the proposed method with the slice manually selected by an expert reader. For each subject, the physical Z-coordinate of both slices was computed in millimeters using the image spatial metadata. This metric directly reflects the accuracy of the proposed slice selection strategy in reproducing the anatomical level typically used in expert-driven TMT assessment.

Figure 7

Qualitative cranial reorientation comparison

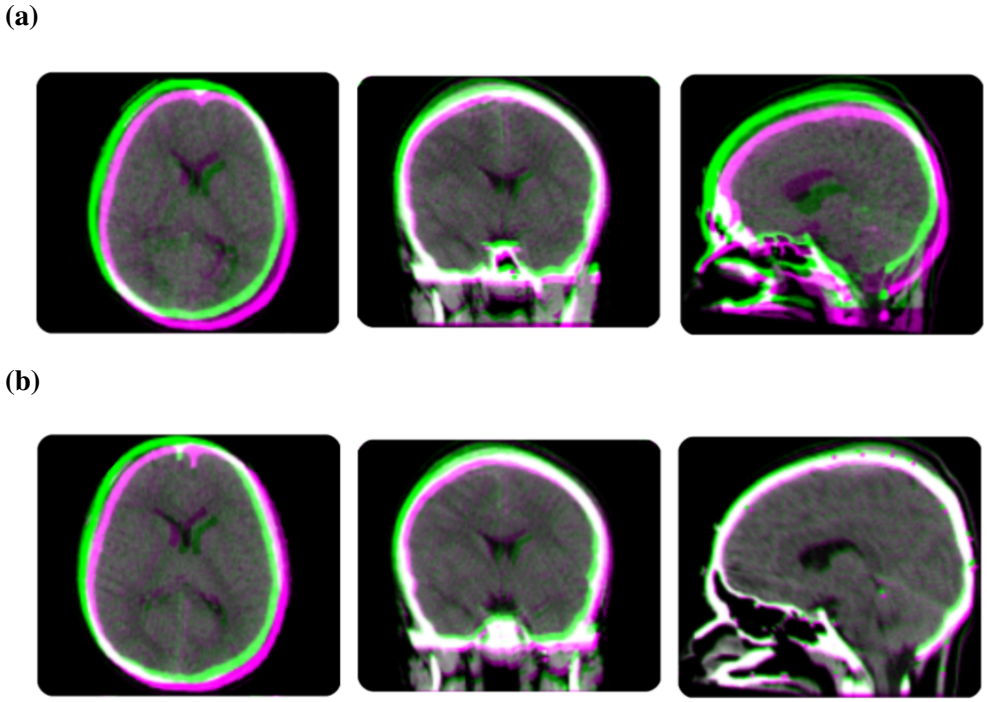

Note. Qualitative comparison of cranial reorientation for a representative subject. (a) Overlay between the original CT volume (green) and the volume manually reoriented by the expert reader (pink). (b) Overlay between the reader-reoriented volume (green) and the volume reoriented using the proposed automated method (pink).

Table 2 summarizes the axial slice position errors across the dataset. The proposed method achieved a median absolute error of 1.92 mm with an interquartile range of 1.21–2.73 mm, indicating close agreement with expert-selected slices. A qualitative visual evaluation was conducted to assess the performance of the proposed automatic axial slice selection method. Figure 8 presents a representative coronal view in which both the automatically and manually selected slices are shown. The proposed method, based on ocular landmark detection and a statistically derived superior offset, identifies a slice that closely matches the selection by the reader.

Table 2

Axial slice selection error

Metric	Median [IQR] (mm)
Axial slice position error	1.92 [1.21 – 2.73]

Note. Absolute Z-axis difference between the automatically selected axial slice and the slice selected by the expert reader. Values are reported as median and interquartile range (IQR).

Figure 8

Manual vs automated axial slice selection

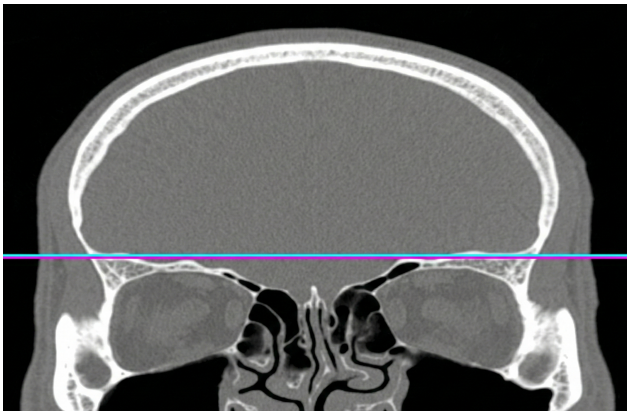

Note. Coronal view illustrating the superposition of the axial slice manually selected by the expert reader (blue) and the slice automatically selected by the proposed method (magenta) for a representative subject.

6.3 Temporalis Muscle Thickness Measurement

The accuracy of the proposed automatic TMT measurement was evaluated by comparison with manual measurements performed by an expert reader on the manually defined axial slices. Absolute TMT errors were computed separately for the left and right sides for each subject.

The proposed method achieved a median absolute error of 1.09 mm with an interquartile range of 0.62–1.68 mm across both sides, indicating close agreement with expert manual measurements. Similar performance was observed for the left and right temporalis muscles individually.

Table 3

Absolute error of automated TMT measurements

Measurement	Median [IQR] (mm)
Left TMT	1.20 [0.65 – 1.75]
Right TMT	1.25 [0.70 – 1.85]
Overall	1.09 [0.62 – 1.68]

Note. Absolute error of automated temporalis muscle thickness (TMT) measurements relative to the expert reader reference. Values are reported as median and interquartile range (IQR).

A qualitative visual evaluation was conducted to assess the anatomical consistency of the proposed TMT measurement strategy. Figure 9 shows a representative axial slice with manual reader measurements (green) overlaid with the automatic measurements obtained by the proposed method (red).

The visual agreement in measurement location, orientation, and extent indicates that the proposed geometry-based approach closely reproduces expert-driven TMT assessment, supporting the quantitative results reported previously.

Figure 9

Qualitative comparison of TMT measurements

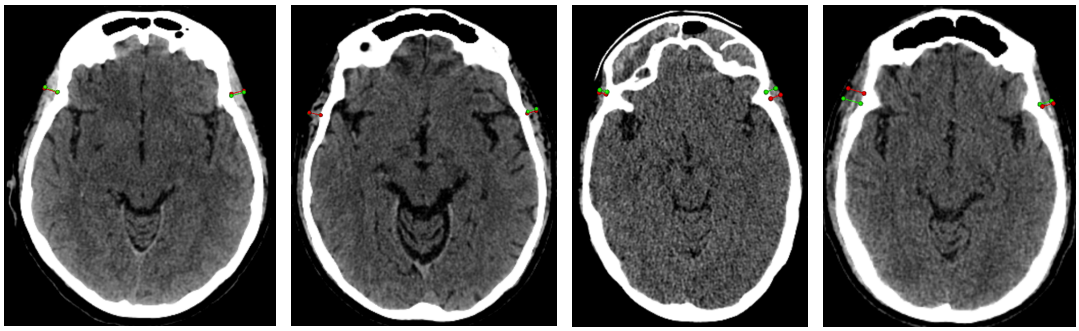

Note. Qualitative comparison of temporalis muscle thickness (TMT) measurements on representative axial CT slices. Manual measurements performed by the expert reader are shown in fluorescent green, whereas automated measurements obtained using the proposed method are shown in red. The overlays demonstrate agreement in anatomical location, measurement orientation, and extent of the temporalis muscle region.

7. Discussion

This work presents a fully automated and deterministic framework for the measurement of temporalis muscle thickness (TMT) from cranial CT volumes, addressing key sources of variability that limit the reliability and reproducibility of manual assessment in clinical practice. Experiments with a dataset of 103 head CT scans demonstrate that the proposed pipeline achieves close agreement with expert reader measurements, with an overall median absolute TMT error of 1.09 mm (IQR: 0.62–1.68 mm) (Table 3), while consistently reproducing the axial slice location typically selected by experts, with a median slice position error of 1.92 mm (Table 2). The observed spatial overlap between automatically selected and expert-selected axial slices along the craniocaudal axis indicates that the proposed approach effectively reproduces expert reader slice selection, supporting its suitability for consistent and fully automated TMT analysis.

When placed in the context of existing literature, the obtained accuracy is comparable to previously reported automated and semi-automated approaches for temporalis muscle analysis. Zapaishchykova *et al.* proposed an automated temporalis muscle quantification framework in MRI, reporting mean absolute errors in the range of 1–2 mm, depending on the age group and acquisition conditions (Zapaishchykova et al., 2023).

More recently, a fully automated volumetric approach for temporalis muscle analysis on head CT was proposed in (Wasserthal et al., 2023). That work demonstrated good agreement with expert measurements and highlighted the potential of three-dimensional muscle characterization for automated TMT assessment. Compared to the proposed method, the volumetric approach offers the advantage of capturing the full three-dimensional extent of the temporalis muscle. However, in routine clinical head CT scans, the inferior origin of the temporalis muscle is rarely included in the field of view, with only the superior two-thirds being consistently available for analysis. As a consequence, volumetric measurements may be incomplete unless this limited anatomical coverage is explicitly considered, which was not addressed in the cited work. In addition, the method does not incorporate an explicit cranial reorientation step to address acquisition-dependent head positioning

variability, and the algorithm is not publicly available.

Learning-based approaches for muscle quantification in CT images, such as those reported by Kanavati *et al.* (Kanavati et al., 2020) and Chen *et al.* (Chen et al., 2025), have demonstrated high segmentation accuracy and strong agreement with expert annotations. Nevertheless, these methods typically rely on large annotated datasets and computationally intensive training procedures, and they are primarily designed for abdominal or whole-body muscle analysis rather than cranial CT or TMT assessment. In contrast, the proposed method relies exclusively on explicit anatomical and geometric constraints, avoiding the need for training data and offering full transparency and interpretability. Our algorithm and the manual annotations by expert readers used in the validation and test sets will be made publicly available.

Our design choice aligns closely with clinical practice, where TMT is measured on a standardized axial slice at the point of maximal muscle thickness rather than through volumetric segmentation. The explicit modeling of anatomical landmarks, slice selection criteria, and geometric measurement rules contribute to the robustness observed across heterogeneous acquisition conditions, including variations in head position, slice thickness, and scanner settings. In addition, the landmark-driven and geometry-based nature of the proposed algorithm provides a high degree of interpretability, allowing clinical specialists to visually inspect intermediate steps, verify measurement locations, and identify potential sources of error. This level of explainability is fundamental for clinical trust and facilitates the adoption of automated TMT assessment in routine practice.

The deterministic nature of the proposed pipeline facilitates reproducible measurements across subjects and time points, which is essential for integrating TMT as a quantitative imaging biomarker in workflows such as nutritional assessment, frailty evaluation, and prognostic stratification. Unlike learning-based approaches, the proposed framework is not expected to be greatly affected by dataset shifts or retraining requirements when applied to new cohorts, further enhancing its potential for real-world clinical deployment.

From a clinical perspective, the reported measurement error is within the range of interobserver variability described for manual TMT assessment. Previous studies have reported interobserver

differences or absolute measurement uncertainties that typically range from approximately 1.0 to 2.0 mm for manual CT-based TMT measurements (Lee et al., 2021; Maskos et al., 2022; Pesonen et al., 2025). For example, Lee *et al.* reported high interobserver agreement when manually measuring TMT on head and neck CT images but also noted millimeter-scale differences attributable to subjective choices in slice selection and boundary delineation (Lee et al., 2021). Similarly, Pesonen *et al.* highlighted that small axial deviations and observer-dependent landmark selection introduce measurable variability in manual TMT measurements (Pesonen et al., 2025). The fact that the proposed method achieves errors within this range suggests that its accuracy is comparable to expert-level manual assessment, supporting its suitability for routine clinical use and longitudinal monitoring.

The main strengths of this study include the fully automated end-to-end design, the use of real-world clinical CT data, and the explicit incorporation of reader-guided anatomical knowledge into both slice selection and measurement. Additionally, the geometry-based formulation ensures interpretability and computational efficiency.

This study has the following limitations. First, the cranial reorientation stage shows limited quantitative improvement when evaluated using absolute axial plane distance (Table 1). While the reduction in median Z-distance after reorientation is moderate, the decreased dispersion of errors indicates improved robustness against extreme acquisition-dependent head orientations. This finding is expected, as the global PCA-based alignment primarily corrects large-scale rotational deviations of the head rather than fine-grained anatomical positioning at the local level. Importantly, this normalization step establishes a consistent spatial reference frame that benefits downstream axial slice selection and TMT measurement, even if it does not fully eliminate residual anatomical offsets. Second, the segmentation strategy relies on fixed intensity thresholds and spatial heuristics, which may be sensitive to severe artifacts or uncommon anatomical variations (Barrett & Keat, 2004).

Future work will focus on improving the anatomical reorientation stage by incorporating more localized or landmark-driven alignment strategies, potentially reducing residual axial discrepancies.

8. Conclusion

In this work, we presented a fully automatic and deterministic method for the measurement of temporalis muscle thickness (TMT) from cranial computed tomography (CT) scans. The proposed approach integrates automatic cranial reorientation, anatomically guided axial slice selection, deterministic tissue segmentation, and a geometry-based thickness estimation strategy that emulates standard measurement practice.

The method was evaluated in a dataset of 148 clinical head CT volumes and demonstrated close agreement with expert reader measurements. A median absolute error of 1.09 mm with an interquartile range of 0.62–1.68 mm was obtained for TMT estimation, while the automatically selected axial slices differed from expert-selected slices by a median of 1.92 mm. These results indicate that the proposed pipeline achieves expert-level accuracy while ensuring full reproducibility and independence from annotated training data.

By relying exclusively on explicit anatomical and geometric constraints, the proposed framework offers a transparent and computationally efficient alternative to learning-based approaches, particularly suited for clinical scenarios where interpretability and robustness are vital. The method enables standardized and scalable TMT assessment and supports the integration of TMT as a quantitative imaging biomarker in both clinical and research workflows.

Future work will focus on improving anatomical reorientation through landmark-based or hybrid alignment strategies, enhancing robustness to imaging artifacts and anatomical variability, validating performance across multi-center datasets, and extending the framework toward three-dimensional temporalis muscle analysis and population-level normative modeling.

References

Altman, D. G. (1991). *Practical statistics for medical research*. Chapman & Hall.

Barrett, J. F., & Keat, N. (2004). Artifacts in ct: Recognition and avoidance. *Radiographics*, *24*(6), 1679–1691. https://doi.org/10.1148/rg.246045065

Bianchi, S., & Martinoli, C. (2007). *Ultrasound of the musculoskeletal system*. Springer.

Bland, J. M., & Altman, D. G. (1986). Statistical methods for assessing agreement between two methods of clinical measurement. *The Lancet*, *327*(8476), 307–310. https://doi.org/10.1016/S0140-6736(86)90837-8

Bonaldi, L., Pretto, A., Pirri, C., Uccheddu, F., Fontanella, C. G., & Stecco, C. (2023). Deep learning-based medical images segmentation of musculoskeletal anatomical structures: A survey of bottlenecks and strategies. *Bioengineering*, *10*(2), 137. https://doi.org/10.3390/bioengineering10020137

Bushberg, J. T., Seibert, J. A., Leidholdt, E. M., & Boone, J. M. (2012). *The essential physics of medical imaging* (3rd ed.). Lippincott Williams & Wilkins.

Chen, Y., Gu, H., Chen, Y., Yang, J., Dong, H., Cao, J. Y., Camarena, A., Mantyh, C., Colglazier, R., & Mazurowski, M. A. (2025). Automated muscle and fat segmentation in computed tomography for comprehensive body composition analysis. *arXiv*. https://doi.org/10.48550/arXiv.2502.09779

Clunie, D. A. (2016). *Dicom structured reporting*. PixelMed Publishing.

Cronin, N. J., Finni, T., & Seynnes, O. R. (2020). Fully automated analysis of muscle architecture from b-mode ultrasound images with deep learning. *arXiv*. https://doi.org/10.48550/arXiv.2009.04790

De Luca, C. J. (1997). The use of surface electromyography in biomechanics. *Journal of Applied Biomechanics*, *13*(2), 135–163. https://doi.org/10.1123/jab.13.2.135

Duda, R. O., & Hart, P. E. (1972). Use of the hough transformation to detect lines and curves in pictures. *Communications of the ACM*, *15*(1), 11–15. https://doi.org/10.1145/361237.361242

Foley, J. D., van Dam, A., Feiner, S. K., & Hughes, J. F. (1996). *Computer graphics: Principles and practice* (2nd ed.). Addison-Wesley.

Gonzalez, R. C., & Woods, R. E. (2018). *Digital image processing* (4th ed.). Pearson.

Hides, J. A., Miokovic, T., Belavy, D. L., Stanton, W. R., & Richardson, C. A. (2007). Ultrasound imaging assessment of abdominal muscle function during drawing-in of the abdominal wall: An intrarater reliability study. *Journal of Orthopaedic and Sports Physical Therapy*, *37*(8), 480–486. https://doi.org/10.2519/jospt.2007.2416

Hsieh, J. (2009). *Computed tomography: Principles, design, artifacts, and recent advances* (2nd ed.). SPIE Press.

Jolliffe, I. T. (2002). *Principal component analysis* (2nd ed.). Springer.

Kak, A. C., & Slaney, M. (2001). *Principles of computerized tomographic imaging*. Society for Industrial; Applied Mathematics (SIAM).

Kanavati, F., Islam, S., Arain, Z., Aboagye, E. O., & Rockall, A. (2020). Fully-automated deep learning slice-based muscle estimation from ct images for sarcopenia assessment. *arXiv*. https://doi.org/10.48550/arXiv.2006.06432

Korfage, J. A. M., Koolstra, J. H., Langenbach, G. E. J., & van Eijden, T. M. G. J. (2005). Fiber-type composition of the human jaw muscles (masseter, temporalis, and pterygoid) based on myosin heavy chain isoforms. *Archives of Oral Biology*, *50*(4), 291–302. https://doi.org/10.1177/154405910508400902

Lee, B., Bae, Y. J., Jeong, W.-J., Kim, H., Choi, B. S., & Kim, J. H. (2021). Temporalis muscle thickness as an indicator of sarcopenia predicts progression-free survival in head and neck squamous cell carcinoma. *Scientific Reports*, *11*(19717). https://doi.org/10.1038/s41598-021-99201-3

Lorensen, W. E., & Cline, H. E. (1987). Marching cubes: A high resolution 3d surface construction algorithm. *ACM SIGGRAPH Computer Graphics*, *21*(4), 163–169. https://doi.org/10.1145/37402.37422

Maskos, A., Schmidbauer, M. L., Kunst, S., Rehms, R., Putz, T., Römer, S., Iankova, V., & Dimitriadis, K. (2022). Diagnostic utility of temporal muscle thickness as a monitoring tool for muscle wasting in neurocritical care. *Nutrients*, *14*(21), 4498. https://doi.org/10.3390/nu14214498

Matsubara, R., Yanagi, Y., Oki, K., Hisatomi, M., Santos, K. C. P., Bamgbose, B. O., Fujita, M., Okada, S., Minagi, S., & Asaumi, J. (2018). Assessment of mri findings and clinical symptoms in patients with temporomandibular joint disorders. *Dentomaxillofacial Radiology*, *47*(4), 20170412. https://doi.org/10.1259/dmfr.20170412

Mohajerani, E., Gümüs, M., Dinger, T. F., Rieß, C., Rauschenbach, L., Rodemerk, J., Ziegenfuß, C. D., Darkwah Oppong, M., Ahmadipour, Y., Li, Y., Dammann, P., Sure, U., & Jabbarli, R. (2025). Temporal muscle thickness as a feasible sarcopenia marker and outcome predictor after aneurysmal subarachnoid hemorrhage. *Acta Neurochirurgica*, *167*, 157. https://doi.org/10.1007/s00701-025-06562-z

Muglia, R., Simonelli, M., Pessina, F., Morenghi, E., Navarria, P., Persico, P., Lorenzi, E., Dipasquale, A., Grimaldi, M., Scorsetti, M., Santoro, A., & Politi, L. S. (2021). Prognostic relevance of temporal muscle thickness as a marker of sarcopenia in patients with glioblastoma at diagnosis. *European Radiology*, *31*(6), 4079–4086. https://doi.org/10.1007/s00330-020-07471-8

Nikkuni, Y., Nishiyama, H., & Hayashi, T. (2018). The relationship between masseter muscle pain and t2 values in temporomandibular joint disorders. *Oral Surgery, Oral Medicine, Oral Pathology and Oral Radiology*, *126*(4), 349–354. https://doi.org/10.1016/j.oooo.2018.06.003

Okeson, J. P. (2019). *Management of temporomandibular disorders and occlusion* (8th ed.). Elsevier.

Pesonen, E. K., Arponen, O., Niinimäki, J., Hernández, N., Pikkarainen, L., Tetri, S., & Korhonen, T. K. (2025). Age- and sex-adjusted ct-based reference values for temporal muscle thickness, cross-sectional area and radiodensity. *Scientific Reports*, *15*(2393). https://doi.org/10.1038/s41598-025-86711-7

Qure.ai. (2018). Non-contrast head/brain ct (cq500) dataset. https://academictorrents.com/details/47e9d8aab761e75fd0a81982fa62bddf3a173831

Soufi, M., Otake, Y., Iwasa, M., Uemura, K., Hakotani, T., Hashimoto, M., Yamada, Y., Yamada, M., Yokoyama, Y., Jinzaki, M., Kusano, S., Takao, M., Okada, S., Sugano, N., & Sato, Y. (2024). Validation of musculoskeletal segmentation model with uncertainty estimation for bone and muscle assessment in hip-to-knee clinical ct images. *arXiv*. https://doi.org/10.48550/arXiv.2409.02770

Standring, S. (Ed.). (2005). *Gray's anatomy: The anatomical basis of clinical practice* (39th ed.). Elsevier Churchill Livingstone.

Steindl, A., Leitner, J., Schwarz, M., Nenning, K.-H., Asenbaum, U., Mayer, S., Woitek, R., Weber, M., Schöpf, V., Berghoff, A. S., Berger, T., Widhalm, G., Prayer, D., Preusser, M., & Furtner, J. (2020). Sarcopenia in neurological patients: Standard values for temporal muscle thickness and muscle strength evaluation. *Journal of Clinical Medicine*, *9*(5), 1272. https://doi.org/10.3390/jcm9051272

Vieira, T. M., & Botter, A. (2021). The accurate assessment of muscle excitation requires the detection of multiple surface electromyograms. *Exercise and Sport Sciences Reviews*, *49*(1), 23–34. https://doi.org/10.1249/JES.0000000000000240

Wasserthal, J., Breit, H.-C., Meyer, M. T., Pradella, M., Hinck, D., Sauter, A. W., Heye, T., Boll, D. T., Cyriac, J., Yang, S., Bach, M., & Segeroth, M. (2023). Totalsegmentator: Robust segmentation of 104 anatomic structures in ct images. *Radiology: Artificial Intelligence*, *5*(5), e230024. https://doi.org/10.1148/ryai.230024

Zapaishchykova, A., Liu, K. X., Saraf, A., Ye, Z., Catalano, P. J., Benitez, V., Ravipati, Y., Jain, A., Huang, J., Hayat, H., Likitlersuang, J., Vajapeyam, S., Chopra, R. B., Familiar, A. M.,

Nabavidazeh, A., Mak, R. H., Resnick, A. C., Mueller, S., Cooney, T. M., . . . Kann, B. H. (2023). Automated temporalis muscle quantification and growth charts for children through adulthood. *Nature Communications*, *14*(6863). https://doi.org/10.1038/s41467-023-42501-1